

Multi-source land-use emissions reveal rising airborne fraction

J. Eduardo Vera-Valdes
Aalborg University, CoRE
eduardo@math.aau.dk

2026-05-23

Abstract The airborne fraction is the share of human carbon dioxide emissions that remains in the atmosphere, and it is a key indicator of how the climate system is responding to continued emissions^{1,2}. Whether this share is rising remains debated because conclusions depend strongly on uncertain estimates of emissions from land-use and land-cover change (LULC). To address this, we use all available LULC measurement series constructed from Global Carbon Budget 2025 data³ and apply a trend framework that explicitly accounts for measurement uncertainty⁴⁻⁶. We show that the airborne fraction has increased over time, and that this conclusion remains when we test sensitivity to excluding the final year and to serial dependence in annual data⁷. These results strengthen evidence that a growing share of emitted carbon dioxide is accumulating in the atmosphere rather than being taken up by land and ocean sinks, with direct implications for carbon-budget assessments and near-term mitigation requirements.

1 Background

2 Whether the airborne fraction (AF) is increasing or approximately constant remains contested^{1,2,8-12}.
3 In its classical form, AF is a yearly ratio of atmospheric growth to total anthropogenic emissions,
4 computed as the sum of fossil fuel emissions and land-use and land-cover change emissions:

$$AF_t = \frac{G_t}{FF_t + LULC_t}, \quad (1)$$

5 where G_t is the annual atmospheric CO_2 growth, FF_t is fossil fuel emissions excluding carbonation,
6 and $LULC_t$ is land-use and land-cover change emissions. AF is a key carbon-cycle diagnostic, with
7 implications for carbon-cycle feedbacks and near-term mitigation planning¹⁻³.
8 A persistent concern is that AF inference depends on the treatment of land-use and land-cover
9 change (LULC) emissions, which are uncertain and model-dependent in annual carbon-budget

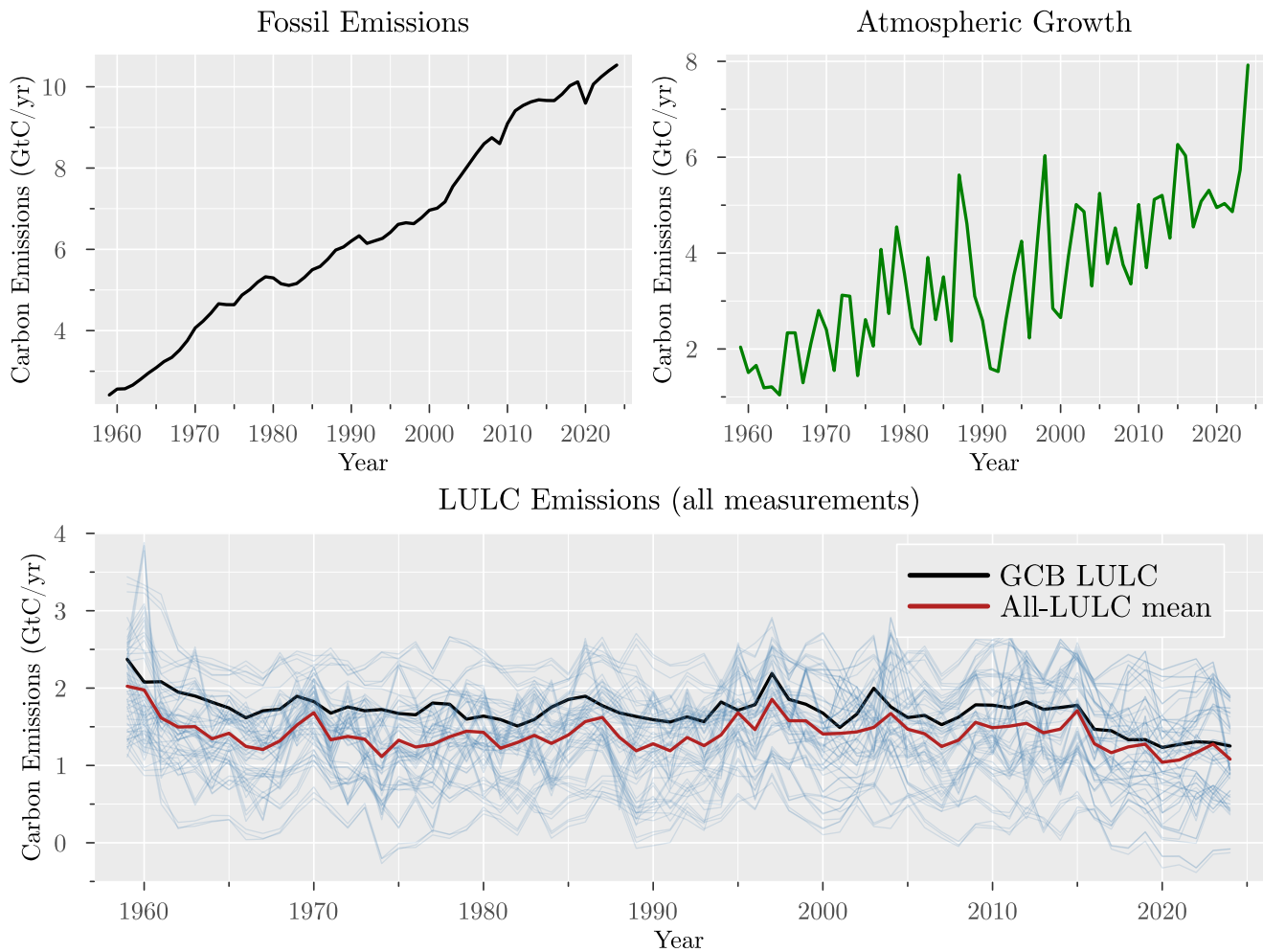
10 accounting³. The Global Carbon Budget (GCB) 2025 dataset provides one column of LULC emissions
11 as the average of three bookkeeping models (BLUE, OSCAR, LUCE), but a broader set of model-based
12 LULC alternatives can be constructed from the same source data. If the information from this broader
13 set of LULC measurements is not incorporated into AF trend inference, tests can be underpowered
14 and inference on trend direction becomes less reliable.

15 Here we address that issue with a design that incorporates measurement uncertainty to obtain more
16 reliable trend estimates⁴⁻⁶. We present a two-stage estimator that propagates denominator
17 uncertainty from repeated LULC measurements into annual AF variance and then estimates the AF
18 trend by weighted least squares (WLS) with heteroskedasticity- and autocorrelation-consistent (HAC)
19 inference⁷. The approach uses cross-measurement dispersion to weight years by precision, rather
20 than treating all years as equally precise as in ordinary least squares (OLS). We find that WLS
21 delivers statistically significant and more stable evidence of positive trend, including under exclusion
22 of the final observation (2024), which shows a large AF jump. For comparison, we estimate OLS on
23 the same AF series, with conventional and HAC standard errors showing weaker evidence of a
24 positive trend and greater sensitivity to endpoint exclusion. This clarifies why evidence based on OLS
25 does not support a clear conclusion about AF trends.

26 **Data**

27 We use annual Global Carbon Budget 2025 data for 1959-2024, with atmospheric growth G_t from
28 NOAA/ESRL global concentration trends¹³, fossil emissions excluding carbonation FF_t from the
29 Global Carbon Project fossil dataset³, and a panel of 69 LULC measurements per year: BLUE¹⁴,
30 OSCAR¹⁵, LUCE¹⁶, and peat-augmented process-based land-model combinations drawn from the GCB
31 model ensemble¹⁷⁻³⁷, combined with peat components³⁸⁻⁴⁰ (see Methods). The data is shown in
32 Figure 1.

33 Two LULC means are constructed from the panel. First, the GCB LULC mean, defined as the mean of
34 the three bookkeeping models BLUE, OSCAR, and LUCE, corresponds to the LULC column used in
35 the Global Carbon Budget. Second, the all-LULC mean, defined as the cross-series mean from all 69
36 LULC measurements. Uncertainty from the multiple LULC measurements are estimated by the cross-
37 measurement dispersion from the full panel.



38
 39 Figure 1: Global Carbon Budget 2025 data for fossil emissions, atmospheric growth, and LULC
 40 emissions (1959-2024). For the LULC panel, we show all extracted and derived LULC measurements
 41 together with the GCB LULC column and the all-LULC cross-series mean.

42 **Identification Strategy**

43 The empirical question is whether AF has a positive linear trend. The key design choice is how to
 44 handle annual denominator uncertainty from multiple LULC measurements. OLS assigns equal
 45 precision to all years and therefore discards information from cross-measurement dispersion. Our
 46 preferred specification uses delta-method variance estimates^{41,42} to construct year-specific weights
 47 and then estimates the trend by WLS, with HAC standard errors for inference^{7,43} (see Methods).

48 Results

49 Full-sample trends

50 Table 1 reports full-sample trend estimates for the four specifications: OLS using GCB LULC, OLS
51 using the all-LULC mean, WLS using the GCB LULC with all-LULC weights, and WLS using the all-
52 LULC mean with all-LULC weights.

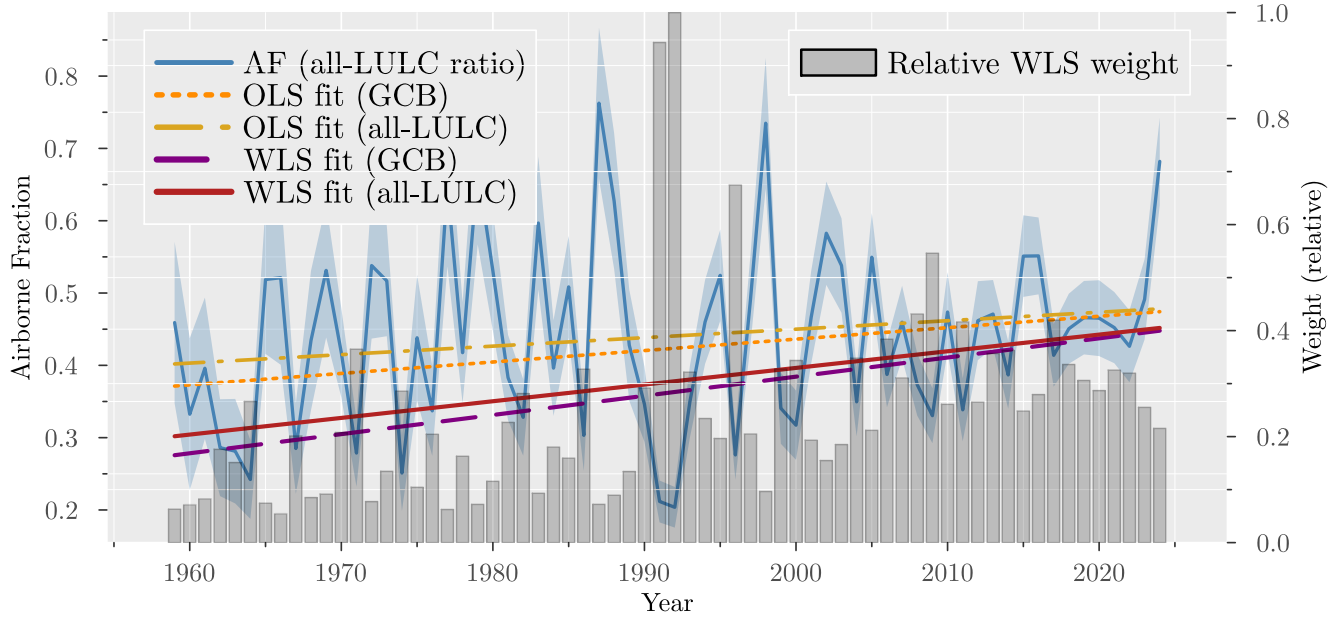
53 Table 1: Full-sample trend comparison across OLS and WLS specifications.

54	Trend, full sample	OLS (GCB)	OLS (all)	WLS (GCB)	WLS (all)
55	Estimate	0.001581	0.001172	0.002649	0.002305
56	Standard error	0.000771	0.000792	0.000022	0.000023
57	HAC standard error	0.000621	0.000643	0.000657	0.000672
58	p-value	0.040212	0.138912	0.000000	0.000000
59	HAC p-value	0.010837	0.068425	0.000056	0.000609
60	R-squared	0.061706	0.033086	0.148987	0.111070

61 The main finding is that incorporating denominator-measurement information via WLS substantially
62 changes inference relative to both OLS benchmarks. In the full sample, all approaches produce a
63 positive slope, and both WLS specifications provide much stronger evidence than OLS (HAC p-values
64 0.000056 and 0.000609 versus 0.010837 and 0.068425). The estimated WLS trend is also steeper
65 (0.002305 per year versus 0.001581 and 0.001172), consistent with greater weight on years with lower
66 denominator uncertainty. The WLS slope implies an increase of about +0.15 in AF over 1959-2024,
67 compared with about +0.10 and +0.08 from the two OLS specifications. The R-squared is also higher
68 for WLS, indicating a better fit when accounting for measurement uncertainty. Nevertheless, the R-
69 squared values are small in absolute terms, signaling that AF is a noisy variable and that the trend is
70 only one component of its variation.

71 Figure 2 shows the AF series using the mean of all LULC measurements together with the associated
72 variance, the OLS trend, and the delta-method WLS trend when using the full sample. The gray bars
73 show the relative weights (standardised so that the maximum weight is 1) assigned to each year in
74 the WLS estimation, which are inversely proportional to the estimated variance of the AF estimate
75 for that year.

Airborne Fraction with OLS and WLS fits for all LULC measurements



76

77 Figure 2: AF series with OLS and delta-method WLS trend (full sample, 1959-2024). Grey bars show
78 the relative weights assigned to each year in the WLS estimation.

79 Note that the WLS trends are steeper than the OLS trends, which is consistent with the numerical
80 results in Table 1. The WLS specifications assign more weight to the more precisely measured years
81 (e.g., 2000-2020 as shown by the width of the shaded area) and less weight to noisier years (e.g.,
82 1960s-1970s), which helps reveal the positive trend signal in the data.

83 **Endpoint Robustness**

84 The final observation (2024) shows a large increase in AF. To ensure this point is not mechanically
85 driving the result, we re-estimate the same four specifications on the subsample ending in 2023.

86 Results are shown in Table 2 and Figure 3.

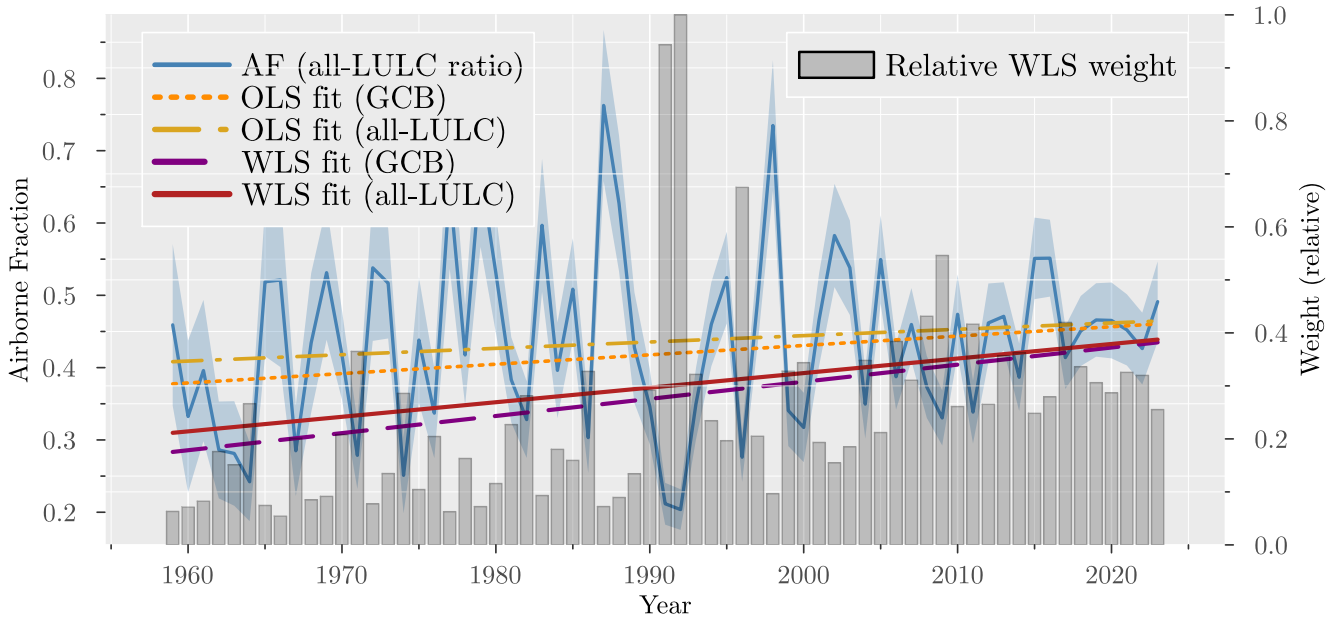
87 Table 2: Subsample (ending in 2023) trend comparison across OLS and WLS specifications.

	Trend (up to 2023)	OLS (GCB)	OLS (all)	WLS (GCB)	WLS (all)
89	Estimate	0.001296	0.000878	0.002367	0.002015
90	Standard error	0.000777	0.000798	0.000022	0.000023
91	HAC standard error	0.000578	0.000600	0.000600	0.000615
92	p-value	0.095163	0.271089	0.000000	0.000000
93	HAC p-value	0.024954	0.143217	0.000081	0.001059
94	R-squared	0.042332	0.018863	0.125521	0.089297

95 Results remain qualitatively unchanged for the WLS specifications: both estimated slopes stay
96 positive and statistically significant (0.002367 with HAC p-value = 0.000081, and 0.002015 with HAC

97 p-value = 0.001059). For the sample ending in 2023, OLS using GCB LULC is positive but only
 98 marginal under conventional inference (p-value = 0.095), while OLS using the all-LULC mean is not
 99 significant (p-value = 0.271). Overall, the WLS results are robust to endpoint exclusion, while OLS
 100 results are more sensitive to denominator construction and provide weaker evidence of a positive
 101 trend.

Airborne Fraction with OLS and WLS fits for all LULC measurements, without 2024



102
 103 Figure 3: AF series with OLS and delta-method WLS trend (sample ending in 2023). Grey bars show
 104 the relative weights assigned to each year in the WLS estimation.

105 **Supplementary Numerical Results**

106 While the main focus is on the slope estimates, we also report intercept estimates for completeness.

107 The intercept captures the baseline AF level in 1959, and its estimation can also be affected by
 108 denominator measurement error.

109 Results for the intercept estimates are shown in Table 3.

110 Table 3: Intercept comparison across OLS and WLS specifications for full sample and sample up to
 111 2023.

112 Intercept	OLS	OLS	WLS	WLS	OLS	OLS	WLS	WLS
113	(GCB)	(all)	(GCB)	(all)	(GCB)	(all)	(GCB)	(all)
114	full	full	full	full	2023	2023	2023	2023
115 Estimate	-2.7266	-1.8946	-4.9141	-4.2130	-2.1611	-1.3121	-4.3539	-3.6377
116 Standard error	1.5352	1.5777	0.0443	0.0456	1.5461	1.5888	0.0440	0.0453
117 HAC standard error	1.2391	1.2845	1.3212	1.3518	1.1553	1.1994	1.2087	1.2390
118 p-value	0.0757	0.2298	0.0000	0.0000	0.1622	0.4089	0.0000	0.0000
119 HAC p-value	0.0278	0.1402	0.0002	0.0018	0.0614	0.2739	0.0003	0.0033
120 R-squared	0.0617	0.0331	0.1490	0.1111	0.0423	0.0189	0.1255	0.0893

121 Discussion and conclusion

122 Using a measurement-error-aware framework, we find robust evidence that AF increased from 1959
 123 to 2024. The key methodological point is that incorporating multi-source denominator uncertainty
 124 through delta-method WLS materially changes inference relative to plain OLS. The endpoint test
 125 shows that this conclusion is not driven by the 2024 jump.

126 In practice, the implication is clear: AF trend assessments should report measurement-error-aware
 127 weighted estimates, benchmark them against OLS, and document endpoint sensitivity.

128 A rising AF implies that a larger share of emitted CO_2 remains in the atmosphere over policy-
 129 relevant horizons, tightening near-term mitigation requirements for a given temperature objective¹⁻³.
 130 The evidence of an increasing AF is consistent with broader findings that the climate system is out of
 131 energy balance and has recently exhibited elevated warming and heating rates; these results should
 132 therefore be interpreted within that wider risk context⁴⁴⁻⁴⁷.

133 Methods

134 Our primary estimator is a two-stage measurement-error trend model using repeated yearly
 135 denominator measurements, followed by weighted trend estimation with HAC inference^{4,5,7,42,43}.

136 Construction of the LULC measurement panel

137 The repeated LULC measurements are built from the Global Carbon Budget 2025 dataset. We first
 138 extract the three bookkeeping series (BLUE, OSCAR, LUCE)¹⁴⁻¹⁶. Then, for each process-based land-
 139 model LULC model in the GCB ensemble which does not already include peat emissions¹⁷⁻³⁷, we add

140 the corresponding peat component to make it comparable to the bookkeeping models, which include
 141 peat emissions by construction. Specifically, for each of the 33 process-based land-model
 142 combinations in the GCB ensemble we create three peat-augmented variants by adding `FAO_peat`,
 143 `LPX_Bern_peat`, and `ORCHIDEE_peat`³⁸⁻⁴⁰. This produces 66 derived series, and together with `BLUE/`
 144 `OSCAR/LUCE` gives a panel of 69 yearly LULC measurements.
 145 In the estimation, the yearly denominator is computed as

$$\hat{C}_t = FF_t + \overline{LULC}_t, \quad \overline{LULC}_t = \frac{1}{n_t} \sum_{j=1}^{n_t} LULC_{tj},$$

146 where $n_t = 3$ for the GCB LULC mean and $n_t = 69$ for the all-LULC mean. The variance of \hat{C}_t is
 147 estimated from the cross-measurement dispersion across the 69 LULC values and is used to construct
 148 the year-specific AF variance estimate used for WLS weighting.

149 Assume for each time $t = 1, \dots, T$ we observe:

- 150 • a single numerator b_t (e.g., atmospheric CO_2 growth), and
- 151 • multiple denominator measurements c_{t1}, \dots, c_{tn_t} with $n_t \geq 2$, which are noisy observations of a
 152 latent C_t .

153 Using the repeated denominator measurements, we can estimate the variance of the ratio estimator
 154 $a_t = b_t/C_t$ via the delta method, which accounts for the variability in C_t due to measurement error.
 155 The procedure is described in detail next.

156 **Two-step estimation approach**

157 We use a two-step approach to estimate the trend in the ratio $a_t = b_t/C_t$ over time, accounting for
 158 denominator measurement error.

159 **Step 1: Estimate C_t and a_t**

- 160 1. Estimate the “true” denominator at time t as the sample mean across available LULC
 161 measurements:

$$\hat{C}_t = \frac{1}{n_t} \sum_{j=1}^{n_t} c_{tj}.$$

162 We consider two variants of this denominator estimate: one using the GCB LULC column (the mean
 163 of `BLUE`, `OSCAR`, `LUCE`) and one using the all-LULC mean (the mean across all 69 LULC
 164 measurements).

165 The variance of \hat{C}_t can be estimated from the multiple measurements.

166 With $n_t \geq 2$, an empirical estimator is

$$\widehat{\text{Var}}(\hat{C}_t) = s_{c,t}^2, \quad s_{c,t}^2 = \frac{1}{n_t - 1} \sum_{j=1}^{n_t} (c_{tj} - \bar{c}_t)^2, \quad \bar{c}_t = \hat{C}_t.$$

167 2. Form the ratio estimate

$$\hat{a}_t = b_t / \hat{C}_t.$$

168 3. Use the multivariate delta method (shown below) to get an approximate variance of \hat{a}_t

$$\widehat{\text{Var}}(\hat{a}_t) \approx \left(\frac{b_t}{\hat{C}_t^2} \right)^2 \widehat{\text{Var}}(\hat{C}_t).$$

169 **Step 2: WLS regression of \hat{a}_t on time**

170 For each time t , we obtain a point estimate \hat{a}_t and an estimated variance $\widehat{\text{Var}}(\hat{a}_t)$ that reflects the

171 cross-measurement dispersion. We use these estimates to fit a linear trend via weighted least squares

172 (WLS):

$$\hat{a}_t = \alpha + \beta t + \varepsilon_t, \quad \varepsilon_t \sim (0, \sigma_t^2), \quad \sigma_t^2 = \widehat{\text{Var}}(\hat{a}_t).$$

173 In our application, the time index t is the year, and \hat{a}_t is the estimated AF for that year. The variance
174 σ_t^2 captures the standard error variance and the uncertainty in the AF estimate due to denominator
175 measurement error, which varies across years depending on the number and variability of the LULC
176 measurements. We use this variance to weight the regression, giving more weight to years with more
177 precise AF estimates.

178 Assuming negligible correlation in ε_t across time, this is WLS with weights $w_t = \frac{1}{\sigma_t^2}$. If we suspect
179 serial correlation, we can use HAC standard errors for inference on β without changing the point
180 estimate. In practice, we use a HAC covariance estimator with a Bartlett kernel and Andrews
181 automatic bandwidth selection⁷. In the results, we report both conventional and HAC standard errors.
182 Testing for a time trend is then a test of $\beta = 0$ versus $\beta \neq 0$ in this linear model, and using WLS we
183 have used all the information in the repeated \hat{a}_t 's through the delta-method approximation.

184 **Delta method for ratio variance estimation**

185 **Step-by-step derivation (first-order delta method):**

186 Define the random vector and the function of interest as

$$X_t = \begin{bmatrix} b_t \\ \hat{C}_t \end{bmatrix}, \quad g(X_t) = \frac{b_t}{\hat{C}_t}.$$

187 and let

$$\sigma_{b,t}^2 = \text{Var} (b_t), \quad \sigma_{C,t}^2 = \text{Var} (\hat{C}_t), \quad \sigma_{bC,t} = \text{Cov} (b_t, \hat{C}_t).$$

188 1. Linearize g around the mean vector $(\mu_{b,t}, \mu_{C,t}) = \mathbb{E}[(b_t, \hat{C}_t)]$:

$$g(X_t) \approx g(\mu_{b,t}, \mu_{C,t}) + \nabla g(\mu_{b,t}, \mu_{C,t})^\top (X_t - \mathbb{E}[X_t]).$$

189 2. Compute the gradient:

$$\nabla g(b, C) = \begin{bmatrix} \partial g / \partial b \\ \partial g / \partial C \end{bmatrix} = \begin{bmatrix} 1/C \\ -b/C^2 \end{bmatrix}.$$

190 3. Write the covariance matrix of (b_t, \hat{C}_t) :

$$\Sigma_t = \begin{bmatrix} \sigma_{b,t}^2 & \sigma_{bC,t} \\ \sigma_{bC,t} & \sigma_{C,t}^2 \end{bmatrix}.$$

191 4. Apply the delta-method variance formula

$$\text{Var} (g(X_t)) \approx \nabla g(\mu_{b,t}, \mu_{C,t})^\top \Sigma_t \nabla g(\mu_{b,t}, \mu_{C,t}),$$

192 and with plug-in evaluation at (b_t, C_t) , this becomes

$$\text{Var} (\hat{a}_t) \approx \left(\frac{1}{C_t} \right)^2 \sigma_{b,t}^2 + \left(\frac{b_t}{C_t^2} \right)^2 \sigma_{C,t}^2 - 2 \frac{b_t}{C_t^3} \sigma_{bC,t}.$$

193 In practice, we use plug-in estimates (replace unknown moments by their empirical counterparts).

194 This is the standard delta-method approximation for the variance of a ratio estimator.

195 5. In the case analysed in this paper, we have a single numerator measurement from a robust source

196 per time, so we treat $\sigma_{b,t}^2$ and $\sigma_{bC,t}$ as negligible relative to the variance from the denominator

197 measurement error, which is captured by $\sigma_{C,t}^2$.

198 The expression simplifies to

$$\text{Var} (\hat{a}_t) \approx \left(\frac{b_t}{C_t^2} \right)^2 \sigma_{C,t}^2.$$

199 Accordingly, a practical plug-in estimator is

$$\widehat{\text{Var}}(\hat{a}_t) \approx \left(\frac{b_t}{\hat{C}_t^2} \right)^2 \widehat{\text{Var}}(\hat{C}_t).$$

200 **Data availability**

201 The study uses publicly available Global Carbon Budget 2025 data and derived yearly series

202 generated from those source files. The processed analysis tables are provided in the repository under

203 the results directory, and the extracted and derived LULC panel is available as a CSV file in the data
204 directory.

205 **Code availability**

206 All code used to process data, estimate models, and generate figures is available in the repository
207 under the scripts directory, including Quarto analysis files and Julia helper functions.

208 **Competing interests**

209 The author declares no competing interests.

210 **Additional information**

211 Supplementary information is not included.

212 **Bibliography**

- 213 1. Canadell, J. G. *et al.* Contributions to accelerating atmospheric CO₂ growth from economic
214 activity, carbon intensity, and efficiency of natural sinks. *Proceedings of the National Academy of*
215 *Sciences* **104**, 18866–18870 (2007).
- 216 2. Raupach, M. R. *et al.* Global and regional drivers of accelerating CO₂ emissions. *Proceedings of*
217 *the National Academy of Sciences* **104**, 10288–10293 (2007).
- 218 3. Friedlingstein, P. *et al.* Global carbon budget 2025. *Earth System Science Data* **18**, 3211–3288
219 (2026).
- 220 4. Fuller, W. A. *Measurement Error Models*. (Wiley, New York, 1987).
- 221 5. Carroll, R. J., Ruppert, D., Stefanski, L. A. & Crainiceanu, C. M. *Measurement Error in Nonlinear*
222 *Models: A Modern Perspective*. (Chapman & Hall/CRC, Boca Raton, 2006).
- 223 6. Vera-Valdés, J. E. & Grivas, C. Robust estimation of carbon dioxide airborne fraction under
224 measurement errors. *Environmental Research Communications* **7**, 31009 (2025).
- 225 7. Newey, W. K. & West, K. D. A Simple, Positive Semi-definite, Heteroskedasticity and
226 Autocorrelation Consistent Covariance Matrix. *Econometrica* **55**, 703–708 (1987).
- 227 8. Knorr, W. Is the airborne fraction of anthropogenic CO₂ emissions increasing?. *Geophysical*
228 *Research Letters* **36**, L21710 (2009).
- 229 9. Ballantyne, A. P., Alden, C. B., Miller, J. B., Tans, P. P. & White, J. W. C. Increase in observed net
230 carbon dioxide uptake by land and oceans during the past 50 years. *Nature* **488**, 70–72 (2012).
- 231 10. Le Quéré, C. *et al.* Trends in the sources and sinks of carbon dioxide. *Nature Geoscience* **2**, 831–
232 836 (2009).

- 233 11. Bennedsen, M., Hillebrand, E. & Koopman, S. J. On the evidence of a trend in the CO₂ airborne
234 fraction. *Nature* **616**, E1–E3 (2023).
- 235 12. Bennedsen, M., Hillebrand, E. & Koopman, S. J. A regression-based approach to the CO₂ airborne
236 fraction. *Nature Communications* **15**, 8507 (2024).
- 237 13. Lan, X., Tans, P. & Thoning, K. W. Trends in globally-averaged CO₂ determined from NOAA
238 Global Monitoring Laboratory measurements. <https://gml.noaa.gov/ccgg/trends/global.html>
239 (2026) doi:10.15138/9N0H-ZH07.
- 240 14. Hansis, E., Davis, S. J. & Pongratz, J. Relevance of methodological choices for accounting of land
241 use change carbon fluxes. *Global Biogeochemical Cycles* **29**, 1230–1246 (2015).
- 242 15. Gasser, T. *et al.* Historical CO₂ emissions from land use and land cover change and their
243 uncertainty. *Biogeosciences* **17**, 4075–4101 (2020).
- 244 16. Qin, Z. *et al.* Global spatially explicit carbon emissions from land-use change over the past six
245 decades (1961-2020). *One Earth* **7**, 835–847 (2024).
- 246 17. Haverd, V. *et al.* A new version of the CABLE land surface model (Subversion revision r4601)
247 incorporating land use and land cover change, woody vegetation demography, and a novel
248 optimisation-based approach to plant coordination of photosynthesis. *Geoscientific Model*
249 *Development* **11**, 2995–3026 (2018).
- 250 18. Melton, J. R. *et al.* CLASSIC v1.0: the open-source community successor to the Canadian Land
251 Surface Scheme (CLASS) and the Canadian Terrestrial Ecosystem Model (CTEM) – Part 1: Model
252 framework and site-level performance. *Geoscientific Model Development* **13**, 2825–2850 (2020).
- 253 19. Lawrence, D. M. *et al.* The Community Land Model version 5: Description of new features,
254 benchmarking, and impact of forcing uncertainty. *Journal of Advances in Modeling Earth Systems*
255 **11**, 4245–4287 (2019).
- 256 20. Fisher, R. A. *et al.* Taking off the training wheels: the properties of a dynamic vegetation model
257 without climate envelopes, CLM4.5(ED). *Geoscientific Model Development* **8**, 3593–3619 (2015).
- 258 21. Tian, H. *et al.* North American terrestrial CO₂ uptake largely offset by CH₄ and N₂O emissions:
259 Toward a full accounting of the greenhouse gas budget. *Climatic Change* **129**, 423–426 (2015).
- 260 22. Ma, L. *et al.* Global evaluation of the Ecosystem Demography model (ED v3.0). *Geoscientific*
261 *Model Development* **15**, 1971–1994 (2022).

- 262 23. Yang, X., Thornton, P., Ricciuto, D., Wang, Y. & Hoffman, F. Global evaluation of terrestrial
263 biogeochemistry in the Energy Exascale Earth System Model (E3SM) and the role of the
264 phosphorus cycle in the historical terrestrial carbon balance. *Biogeosciences* **20**, 2813–2836 (2023).
- 265 24. Needham, J. & others. Vertical canopy gradients of respiration drive plant carbon budgets and
266 leaf area index. *New Phytologist* **246**, 144–157 (2025).
- 267 25. Felzer, B. S. & Jiang, M. Effect of land use and land cover change in context of growth
268 enhancements in the United States since 1700: Net source or sink?. *Journal of Geophysical*
269 *Research: Biogeosciences* **123**, 3439–3457 (2018).
- 270 26. Xia, J. Z. *et al.* The carbon budget of China: 1980–2021. *Science Bulletin* **69**, 114–124 (2024).
- 271 27. Yue, X. *et al.* Development and evaluation of the interactive Model for Air Pollution and Land
272 Ecosystems (iMAPLE) version 1.0. *Geoscientific Model Development* **17**, 4621–4642 (2024).
- 273 28. Shu, S., Jain, A. K., Koven, C. D. & Mishra, U. Estimation of Permafrost SOC Stock and Turnover
274 Time Using a Land Surface Model With Vertical Heterogeneity of Permafrost Soils. *Global*
275 *Biogeochemical Cycles* **34**, e2020GB006585 (2020).
- 276 29. Reick, C. H. *et al.* JSBACH 3 - The land component of the MPI Earth System Model:
277 documentation of version 3.2. (2021) doi:10.17617/2.3279802.
- 278 30. Poulter, B., Frank, D. C., Hodson, E. L. & Zimmermann, N. E. Impacts of land cover and climate
279 data selection on understanding terrestrial carbon dynamics and the CO₂ airborne fraction.
280 *Biogeosciences* **8**, 2027–2036 (2011).
- 281 31. Smith, B. *et al.* Implications of incorporating N cycling and N limitations on primary production
282 in an individual-based dynamic vegetation model. *Biogeosciences* **11**, 2027–2054 (2014).
- 283 32. Schaphoff, S. *et al.* LPJmL4 – a dynamic global vegetation model with managed land – Part 1:
284 Model description. *Geoscientific Model Development* **11**, 1343–1375 (2018).
- 285 33. Lienert, S. & Joos, F. A Bayesian ensemble data assimilation to constrain model parameters and
286 land-use carbon emissions. *Biogeosciences* **15**, 2909–2930 (2018).
- 287 34. Vuichard, N. *et al.* Accounting for carbon and nitrogen interactions in the global terrestrial
288 ecosystem model ORCHIDEE (trunk version, rev 4999): multi-scale evaluation of gross primary
289 production. *Geoscientific Model Development* **12**, 4751–4779 (2019).
- 290 35. Walker, A. P. *et al.* The impact of alternative trait-scaling hypotheses for the maximum
291 photosynthetic carboxylation rate (V_{cmax}) on global gross primary production. *New Phytologist*
292 **215**, 1370–1386 (2017).

- 293 36. Kato, E., Kinoshita, T., Ito, A., Kawamiya, M. & Yamagata, Y. Evaluation of spatially explicit
294 emission scenario of land-use change and biomass burning using a process-based
295 biogeochemical model. *Journal of Land Use Science* **8**, 104–122 (2013).
- 296 37. Ito, A. Disequilibrium of terrestrial ecosystem CO₂ budget caused by disturbance-induced
297 emissions and non-CO₂ carbon export flows: a global model assessment. *Earth System Dynamics*
298 **10**, 685–709 (2019).
- 299 38. Conchedda, G. & Tubiello, F. N. Drainage of organic soils and GHG emissions: validation with
300 country data. *Earth System Science Data* **12**, 3113–3137 (2020).
- 301 39. Müller, J. & Joos, F. Committed and projected future changes in global peatlands – continued
302 transient model simulations since the Last Glacial Maximum. *Biogeosciences* **18**, 3657–3687
303 (2021).
- 304 40. Qiu, C. *et al.* Large historical carbon emissions from cultivated northern peatlands. *Science*
305 *Advances* **7**, eabf1332 (2021).
- 306 41. Cochran, W. G. *Sampling Techniques*. (Wiley, New York, 1977).
- 307 42. Oehlert, G. W. A Note on the Delta Method. *The American Statistician* **46**, 27–29 (1992).
- 308 43. Aitken, A. C. On Least Squares and Linear Combination of Observations. *Proceedings of the Royal*
309 *Society of Edinburgh* **55**, 42–48 (1935).
- 310 44. Minière, A., Schuckmann, K. von, Sallée, J.-B. & Vogt, L. Robust acceleration of Earth system
311 heating observed over the past six decades. *Scientific Reports* **13**, 22975 (2023).
- 312 45. World Meteorological Organization. State of the Global Climate 2025. [https://wmo.int/
313 publication-series/state-of-global-climate/state-of-global-climate-2025](https://wmo.int/publication-series/state-of-global-climate/state-of-global-climate-2025) (2026) doi:10.59327/WMO/
314 S/CRI/SOC/1.
- 315 46. Storto, A. & Yang, C. Acceleration of the ocean warming from 1961 to 2022 unveiled by large-
316 ensemble reanalyses. *Nature Communications* **15**, 545 (2024).
- 317 47. Foster, G. & Rahmstorf, S. Global Warming Has Accelerated Significantly. *Geophysical Research*
318 *Letters* **53**, e2025GL118804 (2026).